LASER & PHOTONICS REVIEWS

www.lpr-journal.org

Nonlinear Exciton-Mie Coupling in Transition Metal Dichalcogenide Nanoresonators

*Anna A. Popkova, Ilya M. Antropov, Gleb I. Tselikov, Georgy A. Ermolaev, Igor Ozerov, Roman V. Kirtaev, Sergey M. Novikov, Andrey B. Evlyukhin, Aleksey V. Arsenin, Vladimir O. Bessonov, Valentyn S. Volkov, and Andrey A. Fedyanin**

Thanks to a high refractive index, giant optical anisotropy, and pronounced excitonic response, bulk transition metal dichalcogenides (TMDCs) have recently been discovered to be an ideal foundation for post-silicon photonics. The inversion symmetry of bulk TMDCs, on the other hand, prevents their use in nonlinear-optical processes such as second-harmonic generation (SHG). To overcome this obstacle and broaden the application scope of TMDCs, MoS_2 nanodisks are engineered to couple Mie resonances with C-excitons. As a result, their alliance produces 23-fold enhancement of SHG intensity with respect to the resonant SHG from a high-quality exfoliated MoS_2 monolayer under C-exciton excitation. Furthermore, SHG demonstrates a strongly anisotropic response typical of a MoS_2 monolayer due to the single-crystal structure of the fabricated nanodisks, providing a polarization degree of freedom to manipulate SHG. Hence, these results significantly improve the potential of bulk TMDCs enabling an avenue for next-generation nonlinear photonics.

1. Introduction

Owing to the enormous potential in post-silicon on-chip technology,[1,2] bulk transition metal dichalcogenides (TMDCs) have emerged from the shadows of monolayer counterparts in recent years. Ultrafast photodetection,[3,4] exciton-polariton transport,[1,5,6] strong coupling,[7,8] Zenneck surface waves,[9] tunable birefringence,[10] anapole modes,[11,12] and ultrasensitive sensors[13,14] are some of the most well-known examples. Superior bulk TMDC characteristics, such as high refractive index,[15] excitonic light–matter interaction,[16] and giant optical anisotropy,[1] lie at the core of these advancements. However, unlike monolayers,[17] inversion symmetry in bulk TMDC leads to negligible quadratic nonlinear optical response, limiting their applications in high harmonic generation,[18] switching,[19] high-resolution imaging,[20] and terahertz generation.[21] As a result, providing a sophisticated optical design for the use of TMDCs in nonlinear processes is critical. Recent studies suggest using different TMDC morphologies, such as nanomesh,[22] tubular,[23] and nanoporous[24] networks. Despite the excellent findings of these studies, these nanostructures are challenging to incorporate into optical circuits.[25] As a result, a new technological approach for TMDC nonlinear integrated nanophotonics is in high demand.

All-dielectric resonant metaphotonics,[26] fortunately, gives a hint to this quest. Manipulation of strong electromagnetic Mie-type resonances in high refractive index nanostructures, for example, considerably amplifies linear[11] and nonlinear[27–31] optical responses of materials. Another advantage of TMDCs is their excitonic nature of dielectric response,[16,32] which greatly enhances light–matter interaction.[33] Specifically, this leads to an increase in harmonic generation due to resonances of nonlinear susceptibilities in the spectral vicinity of excitons both in the monolayer[34,35] and bulk[36] of TMDCs. As a result, combining Mie-type resonances with TMDC excitons could result in significant harmonic generation. Indeed, our findings show that an innovative exciton-Mie coupling regime greatly boosts second-harmonic generation (SHG) in TMDC nanoresonators.

In this work, we designed and fabricated MoS_2 nanodisks, which support Mie-type resonances at the fundamental

A. A. Popkova, I. M. Antropov, V. O. Bessonov, A. A. Fedyanin
Faculty of Physics
Lomonosov Moscow State University
Moscow 119991, Russia
E-mail: fedyanin@nanolab.phys.msu.ru

G. I. Tselikov, G. A. Ermolaev, R. V. Kirtaev, S. M. Novikov, A. B. Evlyukhin, A. V. Arsenin, V. S. Volkov
Center for Photonics and 2D Materials
Moscow Institute of Physics and Technology
9 Institutsky Lane, Dolgoprudny 141700, Russian Federation

I. Ozerov
Aix-Marseille Univ
CNRS
CINAM
Marseille 13288, France

A. B. Evlyukhin
Institute of Quantum Optics
Liebniz University Hannover
Hannover 30167, Germany

A. V. Arsenin, V. S. Volkov
GrapheneTek LLC
Moscow 109004, Russia

V. O. Bessonov
Frumkin Institute of Physical Chemistry and Electrochemistry
Russian Academy of Sciences
Moscow 119071, Russia

The ORCID identification number(s) for the author(s) of this article can be found under https://doi.org/10.1002/lpor.202100604

DOI: 10.1002/lpor.202100604

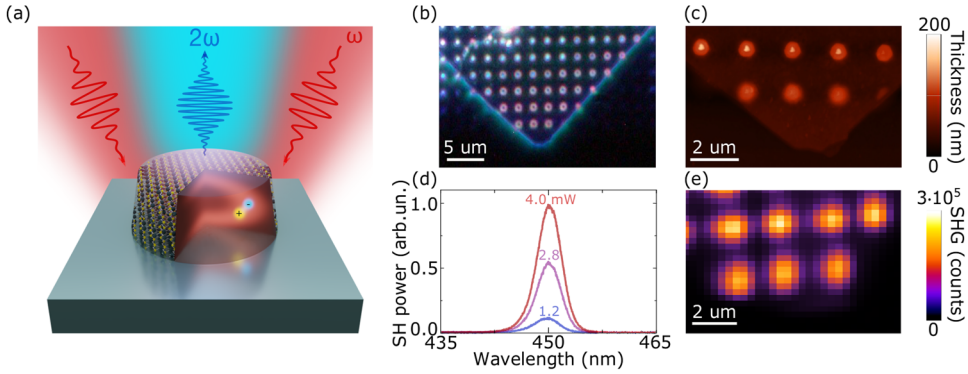

Figure 1. a) Schematic of a MoS_2 nanoresonator and SHG experiment. Pump radiation excites a Mie mode at half the frequency of the exciton resonance of the quadratic susceptibility, thus boosting SHG. b) Optical dark-field microscopy image of the sample with 550 nm nanodisks. c) AFM image of the studied area. d) Spectra of the SH signal from the single 550 nm nanodisk for various pump powers. e) SH intensity map of the studied area with 550 nm MoS_2 nanodisks, measured at a pump wavelength of 900 nm.

wavelength of 900 nm along with the C-exciton resonance at the second-harmonic (SH) wavelength of 450 nm. The proposed system demonstrates the SHG enhancement by more than an order of magnitude in comparison with the maximum achievable intensity of SHG in a MoS_2 monolayer under the C-exciton resonance. Interestingly, SHG exhibits highly anisotropic response, which tentatively originates from hexagonal crystalline structure of fabricated nanodisks. This anisotropic behavior provides an extra degree of freedom to control second-harmonic intensity.[37] Our exciton-Mie approach yields an indispensable route for nonlinear optics in TMDC next-generation photonics.

2. Experimental Samples

A sketch of the system under study is shown in **Figure 1**a. The proposed idea is to excite a Mie-resonance mode in a MoS_2 nanodisk at the fundamental frequency corresponding to half of the MoS_2 C-exciton frequency. In this case, the nonlinear exciton-Mie coupling can be understood from the expression for the SH field: $E_{2\omega} = \chi^{(2)}(2\omega)L^2(\omega)E_{\omega}^2$, where $\chi^{(2)}$ is the MoS_2 quadratic susceptibility depending on the light frequency and L is a local field factor indicating the amplification of the pump field inside the material compared to the incident field E_{ω}. One can dramatically enhance SHG at specific frequency by combining the resonance of the quadratic susceptibility with the Mie-type resonance of the local field factor tailored by the parameters of the nanodisk. We chose the C-exciton resonance, in the spectral vicinity of which the highest value of the quadratic susceptibility has been observed so far for a MoS_2 monolayer,[34] as well as the significant enhancement of SHG has been shown in a centrosymmetric bilayer[38,39] and thin films of MoS_2.[36] The disk shape of nanoresonators allows us to flexibly design resonant modes due to two degrees of freedom: height and diameter. The very high absorption in the spectral region of the C-exciton[1] prevents the excitation of Mie-modes in the nanodisk at the SH frequency and leads to efficient SHG only from the disk's upper layer with a thickness of about 10 nm. Thus, the field of the Mie-mode generating the SH radiation should be localized near the top of the nanodisk. Using numerical simulation by finite difference in time-domain (FDTD) method taking into account the MoS_2 optical anisotropy,[1] we determined that the excitation of the magnetic dipole (MD) mode is accompanied by an increase in the in-plane electric field components at the upper surface of the nanodisk. The disk's height is determined by the height of the MoS_2 flake being 110 nm; thus, the spectral position of the MD resonances was adjusted by changing the disk diameter. For the disk diameter of 550 nm, MD mode is excited at a wavelength of 900 nm corresponding to twice the C-exciton wavelength. As a reference sample, we chose nanodisks with a diameter of 300 nm with an MD resonance observed at the pump wavelength of 800 nm.

MoS_2 nanodisks were fabricated from single-crystal MoS_2 flakes placed on a silicon wafer covered by a 290-nm-thick thermally grown silicon oxide layer. As a fabrication method, we used a well-controlled combination of electron beam lithography and etching with a negative resist as an etching mask allowing us to completely remove the remaining MoS_2 around the disks.

The optical dark-field image of the sample is shown in Figure 1b. Light lines are the boundaries of the etched flake that appeared since the silicon oxide layer outside the flake was overetched simultaneously with MoS_2. Each bright spot inside the boundaries corresponds to a MoS_2 nanodisk. Figure 1c shows the AFM image of the sample. A part of the unwashed resist is seen atop of the disk, which is challenging to remove due to the weak attachment of the MoS_2 flake to the substrate. Using AFM and SEM measurements, we revealed that nanodisks have slightly inclined vertical walls and a shape close to hexagonal, caused by the preferential etching of structures along the armchair crystalline direction.[40] The particle size was determined as the diameter of the inscribed circle at the top of the nanodisk and found to be very close to values determined from the calculation (see Section II, Supporting Information, for details). Nevertheless, the non-circular shape and unwashed resist does not affect the spectral position of the MD resonance and the field distribution inside the nanodisk (see Section IV, Supporting Information). The Raman spectra demonstrate the bulk crystallinity of the fabricated nanodisks (see Section II, Supporting Information). The presence of excitons in MoS_2 nanodisks was confirmed by measuring the reflection spectra of the samples, in which excitons manifest themselves as resonances at 460-, 615-, and 680-nm wavelengths[41] (see Figure S3, Supporting Information).

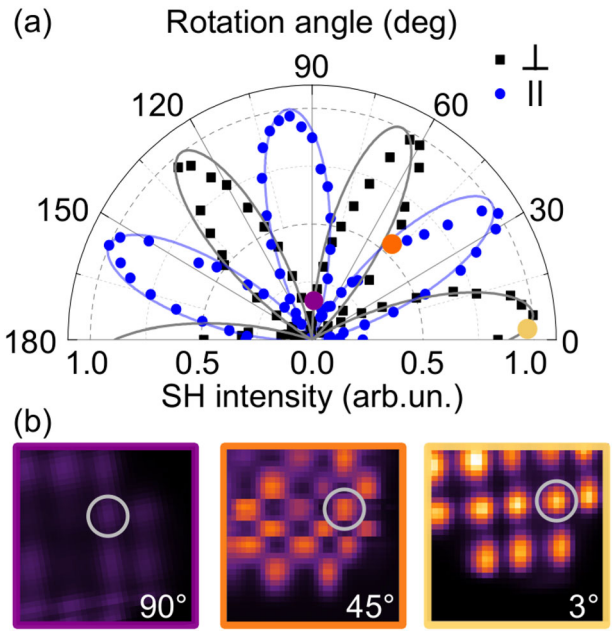

Figure 2. a) Polar plot of the SH intensity measured for the individual nanodisk as a function of the sample azimuthal angle. The polarization of the SHG radiation is parallel (blue dots) and perpendicular (black dots) to the polarization of the pump radiation. Solid curves correspond to the approximation of the experimental data by the $\sin^2(3\phi)$ function, where ϕ is the sample rotation angle. b) SH intensity maps of the same sample area for various azimuthal angles. The gray circle marks the nanodisk, for which the anisotropic dependence is shown in panel (a). Three colored circles in panel (a) indicate the intensity of SHG from marked nanodisk for the cases shown in panel (b).

3. Results and Discussion

The nonlinear optical signal reflected from the sample was measured using a home-built multiphoton microscope based on a femtosecond laser tunable in the spectral range from 680 to 1080 nm (see Section III, Supporting Information, for details).[42] Figure 1d shows spectra of SH intensity generated by a single 550 nm nanodisk measured at various powers of the pump radiation at the fundamental wavelength of 900 nm. The spectra have a peak centered at 450 nm with a width equal to half the width of the pump pulse spectrum[43] and a zero background indicating the absence of multiphoton luminescence and other nonlinear processes in the detected spectral region (see SH spectrum in the wider spectral range in Figure S6, Supporting Information). Figure 1e depicts the SH intensity map of the sample area shown in Figure 1c measured by scanning with a 2-μm-diameter pump beam in increments of 0.3 μm. The SH intensity maxima correspond exactly to the positions of the MoS_2 disks and exceed the SH signal from the substrate by three orders of magnitude.

Nonlinear-optical methods such as SHG are well-suited to find out the symmetry and orientation of crystals. We measured the dependence of the SH intensity on the azimuthal angle of the sample rotation to check whether the crystal structure of MoS_2 was affected during the etching process. The SHG anisotropy dependences for a single MoS_2 nanodisk are shown in **Figure 2**a. Blue and black dots correspond to the parallel and perpendicular orientations of the SH polarization relative to the polarization direction of the pump radiation. Each point of the graph corresponds to the signal from the same disk, measured by scanning the sample for various azimuthal angles. The typical SH scans for several angles are depicted in Figure 2b. The SH intensity from the nanoantenna exhibits strongly varying, sixfold symmetric response as a function of azimuthal angle for both polarizations, that corresponds to the D_{3h} symmetry group of the MoS_2 monolayer.[41] The SH intensity at the minimum is at least two orders of magnitude less than the maximum value, indicating the absence of a significant isotropic contribution. This suggests that the resonators save the crystal structure of MoS_2 during fabrication.

To measure the SH spectra from single MoS_2 nanodisks, we illuminated the samples with wide pump beam 15 μm in diameter and detected a diffraction-limited image of the disk array at the SH wavelength (see Section III, Supporting Information, for details). The SH images obtained at the resonant fundamental wavelengths are shown in **Figure 3**a confirming that SH is generated solely in nanodisks. Figure 3b displays the spectral dependence of the power of SH radiation generated by the disks marked with colored circles in Figure 3a. Black dots show the SH spectrum generated in a MoS_2 monolayer using the 2 μm pump beam with the same fluence as in measurements with nanodisks. For the 550 nm disk, the SH spectrum has the narrow resonance near 900 nm fundamental wavelength. A similar spectral behavior is observed for the MoS_2 monolayer with the SH power being approximately three times smaller. The resonance of SHG from the monolayer is associated with the quadratic susceptibility resonance in the vicinity of the C-exciton.[34] For the disk with a diameter of 300 nm, SH spectrum has two resonances. The spectral position of the long-wavelength resonance corresponds to the C-exciton susceptibility resonance; however, the maximum SH gain is observed at the 800 nm pump wavelength. We measured the linear scattering spectra (Figure 3c) of the same nanodisks to compare the resonances observed in the linear and nonlinear response. For the larger disk, the scattering resonance is revealed near the 900 nm pump wavelength. The scattering spectrum of the smaller disk has the peak near the 800 nm wavelength. The results of FDTD simulation shown by curve in Figure 3c demonstrate good agreement with experimental data and confirm that the observed scattering resonances are associated with the excitation of MD modes in the nanodisks.

We performed numerical simulation for MoS_2 disks of various diameters to trace the spectral shift in the positions of Mie resonances. The calculated scattering cross-section is shown in **Figure 4**a. Analysis of electric and magnetic field distributions together with the results of numerical multipole decomposition[44] allow one to determine the spectral positions of individual Mie resonances. The yellow curve in Figure 4a depicts the dependence of the spectral position of MD resonance on the disk diameter. The field distribution for the 550 nm disk at the 900 nm wavelength is shown in Figure 4b and is typical for the MD mode in nanodisks. A similar fields distribution is observed for the 300 nm disk near the 800 nm wavelength (see Figure S10, Supporting Information). The enhancement of the in-plane field component at the disk surface leads to efficient SHG in the near-surface MoS_2 layers and its emission into free space, while SH generated in the disk volume is absorbed by the material. An example of numerical multipole decomposition for the 550 nm

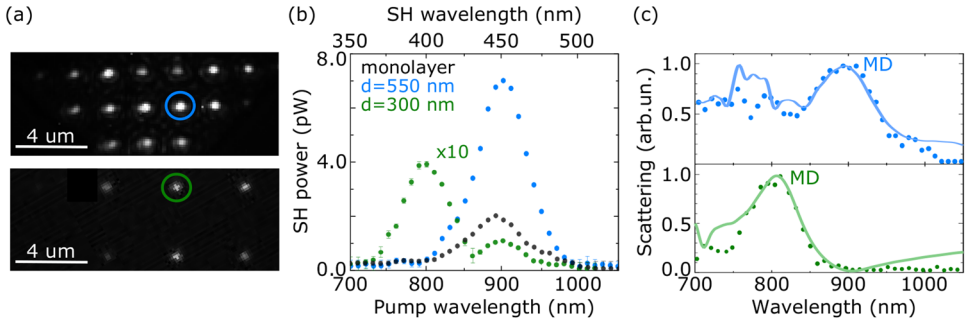

Figure 3. a) SH images of 550 nm (top) and 300 nm (bottom) nanodisks, obtained at 900 and 800 nm pump wavelengths, respectively. Color circles indicate the nanodisks, the SHG, and scattering spectra of which are shown in panels (b) and (c). b) SHG spectra of MoS_2 nanodisks (color dots) and monolayer (black dots) measured at 16 GW cm^{-}2 peak intensity corresponding to the 5 mW pump power for 2 μm focused beam. c) Measured (dots) and calculated (curves) scattering spectra of the MoS_2 nanodisks with a diameter of 550 nm (top) and 300 nm (bottom).

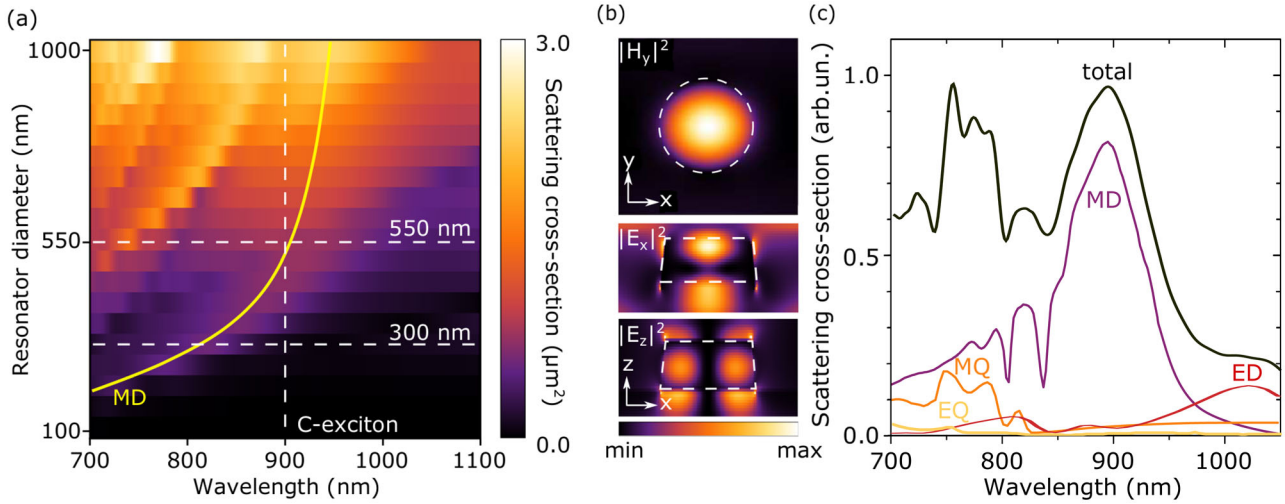

Figure 4. a) Spectra of scattering cross-section calculated for various disk diameters. Yellow curve shows the position of the MD resonance. The dashed lines indicate the sizes of the experimental nanodisks and doubled C-exciton wavelength. b) Electric and magnetic field distributions in the 550 nm nanodisk at the 900 nm pump wavelength. Dashed curve indicates the disk boundaries. c) Result of numerical multipole decomposition of scattering cross-section for the 550 nm nanodisk.

nanodisk shown in Figure 4c demonstrates the sole contribution of MD resonance to the optical response in the vicinity of the doubled C-exciton wavelength. Note, that in the short-wavelength region, the sum of the contributions of the calculated multipoles is less than the total scattering cross section. This is explained by the contributions to scattering from the Si/SiO_2 substrate, higher order multipoles (octupoles, etc.), as well as possible Fabry–Pérot modes, which are not taken into account in the calculations. Nevertheless, a comparison of the numerical decomposition with the more rigorous analytical multipole decomposition performed by the discrete dipoles method[45,46] for a MoS_2 nanodisk in vacuum shows good agreement between the spectral positions of the Mie resonances (see Section IV, Supporting Information).

The measured SH signal from monolayer allows us to estimate the second-order nonlinear optical susceptibility of MoS_2 at C-exciton resonance. Using the method described in ref. [47], we obtain $\chi^{(2)}$=220 pm V^{-1} (see Section V, Supporting Information) that is in a good agreement with previously reported one.[34] This value can be slightly underestimated due to the complex structure of the substrate (see Section V, Supporting Information, for details). Using MoS_2 monolayer as a reference, we can estimate the gain in the nonlinear response of nanodisks. To do this correctly, we must take into account the area of the SHG sources and obtain the SH intensity for each sample. For a disk, the SH source area can be estimated as the area of the disk's upper face, measured using scanning electron microscopy or AFM. In the case of monolayer, the SH source area is the pump spot area divided by $\sqrt{2}$. The spectral dependences of the SH intensity are shown in **Figure 5**, where the maximum value of intensity for the MoS_2 monolayer is taken as the unity. The SH intensity gain for the 300 nm disk is approximately 5 when the MD mode is excited. The enhancement of the intensity at the wavelength of the C-exciton coincides in amplitude with the monolayer one. For double-resonant sample, the maximum SHG gain of 23 is observed at the 900 nm wavelength that corresponds to the overlap of MD resonance and C-exciton. It is worth noting that the observed gain value of 23 ± 1 is repeated with good accuracy for a set of disks having the same geometric parameters (see

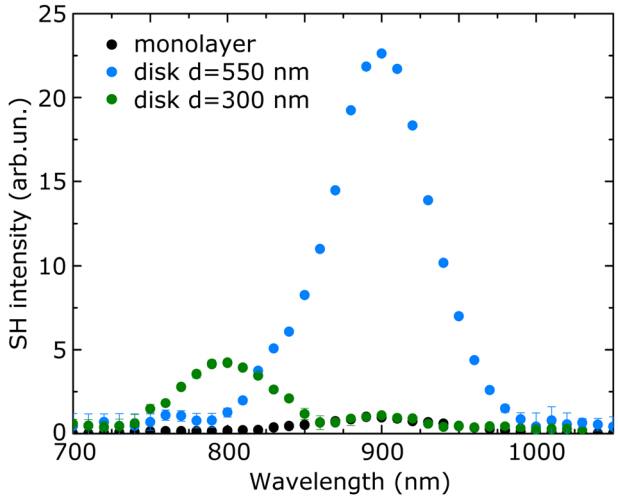

Figure 5. SH intensity spectra for the 550 nm (blue) and 300 nm (green) MoS_2 nanodisks and MoS_2 monolayer (black). The maximum intensity of SHG from monolayer at C-exciton resonance is taken as unity.

Section VII, Supporting Information, for details). In this case, the intensity is 10^3 times greater than that generated in the MoS_2 monolayer away from the C-exciton resonance. The experimental conversion coefficient is 5×10^{-7} W^{-1}. Taking into account that only 25% of the pump power hits the nanodisk surface, the actual SH efficiency can be estimated as 2×10^{-6} W^{-1}. The observed values of the gain and conversion coefficients are comparable with the ones obtained using optomechanical amplification of the SH signal,[48] as well as the combination of a MoS_2 monolayer with a micro-cavity[49] and bound state in the continuum[50] systems. Also, the demonstrated efficiency is two orders of magnitude larger than the SH conversion efficiency for a MoS_2 metasurface with Mie resonances[51] in the absence of absorption at the SH frequency.

Using a simple model (see Section IV, Supporting Information) and taking into account that only the upper 20–30 MoS_2 layers contribute to the measured SH, we roughly estimated the bulk quadratic susceptibility of MoS_2 forming nanodisks as 70% of the monolayer susceptibility, which is a surprising result for nominally centrosymmetric medium. The question of a possible origin of SHG in TMDC-based centrosymmetric structures is still debatable, and evidence is demonstrated both in favor of a bulk contribution[12] and a strictly surface one.[51] While in most works the centrosymmetric nature is demonstrated by the absence of SHG from MoS_2 films with an even number of layers,[34,41,52] in several works, a significant enhancement of SHG from a bilayer compared to a monolayer was revealed by tuning SH wavelength to exciton resonance.[38,39] The intensity of SHG from the bilayer was shown to reach more than 10% of the one from the monolayer demonstrating the sixfold anisotropic dependence, which was associated with the breaking of inverse symmetry due to built-in electric fields.[39] We have measured the SHG anisotropic dependences for our MoS_2 monolayer and bilayer at 900 nm pump wavelength under the same experimental conditions and found that the intensity of the SH from the bilayer is 5% of monolayer one and shows the same sixfold symmetry (see Section VIII, Supporting Information), in accordance with ref. [39]. Since the absorption of MoS_2 monolayer at C-exciton resonance reaches 5%, we can also assume an additional mechanism for SHG enhancement in bilayer, which consists of the uncompensated destructive interference of the SH waves from the upper and lower layers due to the partial absorption of SH wave from the lower layer by the upper layer. Thus, the large SH signal from nanodisks observed in our experiment may be considered as the result of constructive interference of weak uncompensated dipole contributions from 10–15 closely spaced bilayers in the upper part of the nanodisk. The dipole bulk nature of SHG in our case of C-exciton excitation confirms the experimentally observed anisotropic dependence for nanodisks, which is similar to that from MoS_2 monolayer. At the same time, the considered mechanism does not contradict the results of ref. [51], since SH radiation was not absorbed in their system resulting in perfect cancellation of dipole contributions from adjacent layers in the MoS_2 bulk.

4. Conclusion

In conclusion, the high refractive index of bulk TMDCs, along with the presence of excitons at room temperature, allows creating a nanoresonator with a significantly enhanced non-linear optical response. Here, thanks to flexible adjusting of Mie-resonance modes, we have coupled the exciton resonance of the MoS_2 quadratic susceptibility with the MD resonance through a nonlinear optical process of SHG. By etching a single-crystal MoS_2 flake, nanodisks were fabricated to support the MD mode at a wavelength of 900 nm corresponding to the doubled C-exciton wavelength. As the result, the intensity of SH generated by the nanodisks exceeded the intensity of SHG from MoS_2 monolayer at the C-exciton resonance by a factor of 23 ± 1. Single-crystal nanodisks exhibit sixfold anisotropic SHG, similar to the monolayer case, which is an additional knob in controlling the SH radiation. A variety of subwavelength geometrical modes and their interplay in nanoresonators[27,53,54] can be used to further enhance the exciton-mediated nonlinear response. In turn, the electrical control of the exciton-enhanced quadratic susceptibility[19,38,39] paves the way toward a new tunable nonlinear nanophotonic devices based on TMDCs.

5. Experimental Section

Sample Fabrication: Arrays of MoS_2 nanoresonators were fabricated by electron beam lithography (EBL) followed by reactive ion etching (RIE). The substrates cleaved from silicon (100) wafers covered by a 290-nm-thick thermally grown silicon oxide were used. The substrates were pre-patterned by optical lithography in order to facilitate the identification of areas for the following MoS_2 deposition. First, the substrates were cleaned in sequential ultrasonic bathes of acetone and isopropanol, rinsed in deionized water, and dried under clean nitrogen flow. Then, the substrates were exposed to the oxygen radical plasma treatment in a barrel reactor (Nanoplas, France). MoS_2 flakes were deposited on substrates using mechanical exfoliation from highly oriented synthetic 2H-phase MoS_2 crystal (2D Semiconductors Inc., USA) (Figure S1a, Supporting Information). The flakes to pattern were chosen under an optical microscope, and their thicknesses were measured by a contact profilometer (DektakXT, Bruker, Germany). The flakes with a thickness of 110 nm and a lateral size of about 100 μm × 50 μm were chosen for further patterning. A negative tone electron beam resist (ARN 7520.18 from Allresist, Germany) was spin-coated

on the sample at a speed of 4000 rpm and pre-baked on a 85 °C hotplate for 5 min (measured thickness 469 nm). A conductive polymer (AR-PC 5091.02 from Allresist) layer was successively spin-coated in order to prevent the surface charging during e-beam exposure. Then, an EBL tool (Pioneer, Raith, Germany) was used for sample patterning (Figure S1b, Supporting Information). We used 21 kV acceleration voltage of the electron gun, and the beam current was 0.24 nA for the aperture of 30 μm. The typical write field was 500 μm, and the nominal exposition dose was 1000 μC cm−2. The pattern represented a square array of 50 × 50 dots with a period between dots of 2 or 4 μm. After the exposure, the conductive resist was rinsed off in pure deionized water, and the negative tone resist was developed in a AR 300-47 solution containing tetramethylammonium hydroxide. The next step was to etch pillars into MoS_2 by RIE in SF_6 (ICPE Corial 200I) at 100 W power at 10 mTorr working pressure with a flow of 50 sccm using the patterned photoresist as a mask (Figure S1c, Supporting Information). The etching rate of MoS_2 was evaluated as 100 nm min^{-1} by comparison with the reference nonpatterned MoS_2 flake of known thickness. The etching time was adjusted to completely etch MoS_2 between the pillars. Finally, the resist was removed in a corresponding organic solvent solution. Figure S1, Supporting Information, shows SEM images of the flakes with visible disk-like nanoresonators after fabrication.

Experimental Setup: The nonlinear signal from the sample was detected using a home-built multiphoton microscope based on the femtosecond laser (Coherent Chameleon, 150 fs pulse duration, 80 MHz repetition rate) tunable in the spectral range from 680 to 1080 nm. Registration of the SH signal reflected from the sample was made in two ways. First, the laser beam was focused at the sample surface and reflected SH signal was measured by a monochoromator and CCD camera (Andor Clara) to record the spectrum of the nonlinear response. Second, we used a kind of Köhler illumination scheme by installing an additional lens in the pump channel and observing an SH image of the sample from a large surface area on a CMOS camera (Photometrics Prime). The precise position of the sample relative to the pump spot was controlled by a three-axis motorized stage. The modification of nonlinear setup also allowed to measure linear scattering and reflection spectra at fundamental wavelengths without manipulating the sample. The detailed description is given in Section III, Supporting Information.

Numerical Simulation: The numerical simulation of scattering cross-section and electromagnetic field distribution was performed by FDTD method in Lumerical software. The calculated system consisted of a MoS_2 disk on a silicon substrate covered with a 290-nm-thick layer of silicon oxide. The in-plane and out-of-plane refractive indexes of MoS_2 were taken from ref. [1]. The multipole mode decomposition of the scattering radiation was performed by numerical integration of the total electric field induced by a normally incident plane wave inside the nanoantenna.[44] The multipole mode decomposition for MoS_2 disk in free space was performed by discrete dipolar approximation technique.[45,46]

Supporting Information

Supporting Information is available from the Wiley Online Library or from the author.

Acknowledgements

The authors sincerely thank Frédéric Bedu for his help with nanofabrication processes performed at PLANETE cleanroom facility (CINaM, Marseille). The work was performed under partial financial support of the Russian Ministry of Education and Science (Grant No. 14.W03.31.0008), the Russian Science Foundation (grant No. 21-19-00675, sample design and fabrication; grant No. 21-79-00206, linear optical characterization; grant No. 20-12-00371, nonlinear-optical measurements), and Russian Foundation for Basic Research (grant No.21-52-12036, numerical simulations). Part of the research was supported by MSU Quantum Technology Centre and the Development program of the MSU Interdisciplinary Scientific and Educational School "Photonic and Quantum technologies. Digital Medicine". The support from the Deutsche Forschungsgemeinschaft (DFG, German Research Foundation) under Germany's Excellence Strategy within the Cluster of Excellence PhoenixD (EXC 2122, Project ID 390833453) is acknowledged. A.A.P. acknowledges support by "BASIS" Foundation (grant No. 19-2-6-28-1). G.A.E. acknowledges support by grant of the President of Russian Federation to young scientists and postgraduates.

Conflict of Interest

The authors declare no conflict of interest.

Data Availability Statement

The data that support the findings of this study are available from the corresponding author upon reasonable request.

Keywords

excitons, Mie resonances, molybdenum disulfide, second-harmonic generation, transition metal dichalcogenides

Received: October 25, 2021
Revised: January 16, 2022
Published online: March 6, 2022

[1] G. A. Ermolaev, D. V. Grudinin, Y. V. Stebunov, K. V. Voronin, V. G. Kravets, J. Duan, A. B. Mazitov, G. I. Tselikov, A. Bylinkin, D. I. Yakubovsky, S. M. Novikov, D. G. Baranov, A. Y. Nikitin, I. A. Kruglov, T. Shegai, P. Alonso-González, A. N. Grigorenko, A. V. Arsenin, K. S. Novoselov, V. S. Volkov, *Nat. Commun.* **2021**, *12*, 854.
[2] H. Ling, R. Li, A. R. Davoyan, *ACS Photonics* **2021**, *8*, 721.
[3] N. Flöry, P. Ma, Y. Salamin, A. Emboras, T. Taniguchi, K. Watanabe, J. Leuthold, L. Novotny, *Nat. Nanotech.* **2020**, *15*, 118.
[4] Y. Chen, Y. Wang, Z. Wang, Y. Gu, Y. Ye, X. Chai, J. Ye, Y. Chen, R. Xie, Y. Zhou, Z. Hu, Q. Li, L. Zhang, F. Wang, P. Wang, J. Miao, J. Wang, X. Chen, W. Lu, P. Zhou, W. Hu, *Nat. Electron.* **2021**, *4*, 357.
[5] F. Hu, Y. Luan, J. Speltz, D. Zhong, C. Liu, J. Yan, D. Mandrus, X. Xu, Z. Fei, *Phys. Rev. B* **2019**, *100*, 121301.
[6] F. Hu, Y. Luan, M. Scott, J. Yan, D. Mandrus, X. Xu, Z. Fei, *Nat. Photon.* **2017**, *11*, 356.
[7] B. Munkhbat, D. G. Baranov, M. Stührenberg, M. Wersäll, A. Bisht, T. Shegai, *ACS Photonics* **2018**, *6*, 139.
[8] C.-H. Liu, I. S. Kim, L. J. Lauhon, *Nano Lett.* **2015**, *15*, 6727.
[9] V. E. Babicheva, S. Gamage, L. Zhen, S. B. Cronin, V. S. Yakovlev, Y. Abate, *ACS Photonics* **2018**, *5*, 2106.
[10] D. Hu, K. Chen, X. Chen, X. Guo, M. Liu, Q. Dai, *Adv. Mater.* **2019**, *31*, 1807788.
[11] R. Verre, D. G. Baranov, B. Munkhbat, J. Cuadra, M. Käll, T. Shegai, *Nature Nanotech.* **2019**, *14*, 679.
[12] S. Busschaert, R. Reimann, M. Cavigelli, R. Khelifa, A. Jain, L. Novotny, *ACS Photonics* **2020**, *7*, 2482.
[13] G. Ermolaev, K. Voronin, D. G. Baranov, V. Kravets, G. Tselikov, Y. Stebunov, D. Yakubovsky, S. Novikov, A. Vyshnevyy, A. Mazitov, I. Kruglov, S. Zhukov, R. Romanov, A. M. Markeev, A. Arsenin, K. S. Novoselov, A. N. Grigorenko, V. Volkov, *arXiv preprint arXiv:2106.12390* **2021**.
[14] H. Hu, A. Zavabeti, H. Quan, W. Zhu, H. Wei, D. Chen, J. Z. Ou, *Biosens. Bioelectron.* **2019**, *142*, 111573.
[15] G. A. Ermolaev, Y. V. Stebunov, A. A. Vyshnevyy, D. E. Tatarkin, D. I. Yakubovsky, S. M. Novikov, D. G. Baranov, T. Shegai, A. Y. Nikitin, A. V. Arsenin, V. S. Volkov, *npj 2D Mater. Appl.* **2020**, *4*, 21.

[16] Y. Yu, Y. Yu, Y. Cai, W. Li, A. Gurarslan, H. Peelaers, D. E. Aspnes, C. G. Van de Walle, N. V. Nguyen, Y.-W. Zhang, L. Cao, *Sci. Rep.* **2015**, *5*, 16996.
[17] A. Säynätjoki, L. Karvonen, H. Rostami, A. Autere, S. Mehravar, A. Lombardo, R. A. Norwood, T. Hasan, N. Peyghambarian, H. Lipsanen, K. Kieu, A. C. Ferrari, M. Polini, Z. Sun, *Nat. Commun.* **2017**, *8*, 893.
[18] H. Liu, Y. Li, Y. S. You, S. Ghimire, T. F. Heinz, D. A. Reis, *Nat. Phys.* **2017**, *13*, 262.
[19] K. L. Seyler, J. R. Schaibley, P. Gong, P. Rivera, A. M. Jones, S. Wu, J. Yan, D. G. Mandrus, W. Yao, X. Xu, *Nat. Nanotechnol.* **2015**, *10*, 407.
[20] L. Olivieri, J. S. T. Gongora, L. Peters, V. Cecconi, A. Cutrona, J. Tunesi, R. Tucker, A. Pasquazi, M. Peccianti, *Optica* **2020**, *7*, 186.
[21] L. Hu, D. Wei, X. Huang, *J. Chem. Phys.* **2017**, *147*, 244701.
[22] A. W. Murphy, Z. Liu, A. V. Gorbach, A. Ilie, V. K. Valev, *Laser Photonics Rev.* **2021**, *15*, 2100117.
[23] R. Xiang, T. Inoue, Y. Zheng, A. Kumamoto, Y. Qian, Y. Sato, M. Liu, D. Tang, D. Gokhale, J. Guo, K. Hisama, S. Yotsumoto, T. Ogamoto, H. Arai, Y. Kobayashi, H. Zhang, B. Hou, A. Anisimov, M. Maruyama, Y. Miyata, S. Okada, S. Chiashi, Y. Li, J. Kong, E. I Kauppinen, Y. Ikuhara, K. Suenaga, S. Maruyama, *Science* **2020**, *367*, 537.
[24] B. Zheng, Y. Chen, Z. Wang, F. Qi, Z. Huang, X. Hao, P. Li, W. Zhang, Y. Li, *2D Mater.* **2016**, *3*, 035024.
[25] W. Bogaerts, D. Pérez, J. Capmany, D. A. Miller, J. Poon, D. Englund, F. Morichetti, A. Melloni, *Nature* **2020**, *586*, 207.
[26] J. Xu, Y. Wu, P. Zhang, Y. Wu, R. A. Vallée, S. Wu, X. Liu, *Adv. Opt. Mater.* **2021**, *9*, 2100112.
[27] K. Koshelev, S. Kruk, E. Melik-Gaykazyan, J.-H. Choi, A. Bogdanov, H.-G. Park, Y. Kivshar, *Science* **2020**, *367*, 288.
[28] R. Colom, L. Xu, L. Marini, F. Bedu, I. Ozerov, T. Begou, J. Lumeau, A. E. Miroshnishenko, D. Neshev, B. T. Kuhlmey, S. Palomba, N. Bonod, *ACS Photoics* **2019**, *6*, 1295.
[29] M. R. Shcherbakov, D. N. Neshev, B. Hopkins, A. S. Shorokhov, I. Staude, E. V. Melik-Gaykazyan, M. Decker, A. A. Ezhov, A. E. Miroshnichenko, I. Brener, A. A. Fedyanin, Y. S. Kivshar, *Nano Lett.* **2014**, *14*, 6488.
[30] M. K. Kroychuk, D. F. Yagudin, A. S. Shorokhov, D. A. Smirnova, I. I. Volkovskaya, M. R. Shcherbakov, G. Shvets, Y. S. Kivshar, A. A. Fedyanin, *Adv. Opt. Mater.* **2019**, *7*, 1900447.
[31] L. Shi, A. B. Evlyukhin, C. Reinhardt, I. Babushkin, V. A. Zenin, S. Burger, R. Malureanu, B. N. Chichkov, U. Morgner, M. Kovacev, *ACS Photonics* **2020**, *7*, 1655.
[32] G. A. Ermolaev, D. I. Yakubovsky, Y. V. Stebunov, A. V. Arsenin, V. S. Volkov, *J. Vac. Sci. Technol. B* **2020**, *38*, 014002.
[33] S. B. Anantharaman, K. Jo, D. Jariwala, *ACS Nano* **2021**, *15*, 12628.
[34] L. M. Malard, T. V. Alencar, A. P. M. Barboza, K. F. Mak, A. M. de Paula, *Phys. Rev. B* **2013**, *87*, 201401.
[35] G. Wang, X. Marie, I. Gerber, T. Amand, D. Lagarde, L. Bouet, M. Vidal, A. Balocchi, B. Urbaszek, *Phys. Rev. Lett.* **2015**, *114*, 097403.
[36] M. L. Trolle, Y.-C. Tsao, K. Pedersen, T. G. Pedersen, *Phys. Rev. B* **2015**, *92*, 161409.
[37] S. Klimmer, O. Ghaebi, Z. Gan, A. George, A. Turchanin, G. Cerullo, G. Soavi, *Nat. Photon.* **2021**, *15*, 837.
[38] J. Klein, J. Wierzbowski, A. Steinhoff, M. Florian, M. Rösner, F. Heimbach, K. Müller, F. Jahnke, T. O. Wehling, J. J. Finley, M. Kaniber, *Nano Lett.* **2017**, *17*, 392.
[39] S. Shree, D. Lagarde, L. Lombez, C. Robert, A. Balocchi, K. Watanabe, T. Taniguchi, X. Marie, I. C. Gerber, M. M. Glazov, L. E. Golub, B. Urbaszek, I. Paradisanos, *Nat. Commun.* **2021**, *12*, 6894.
[40] B. Munkhbat, A. B. Yankovich, D. G. Baranov, R. Verre, E. Olsson, T. O. Shegai, *Nat. Commun.* **2020**, *11*, 4604.
[41] Y. Li, Y. Rao, K. F. Mak, Y. You, S. Wang, C. R. Dean, T. F. Heinz, *Nano Lett.* **2013**, *13*, 3329.
[42] A. A. Popkova, I. M. Antropov, J. E. Fröch, S. Kim, I. Aharonovich, V. O. Bessonov, A. S. Solntsev, A. A. Fedyanin, *ACS Photonics* **2021**, *8*, 824.
[43] S. A. Akhmanov, V. A. Vysloukh, A. S. Chirkin, *Optics of Femtosecond Laser Pulses*, AIP, New York **1992**.
[44] R. Alaee, C. Rockstuhl, I. Fernandez-Corbaton, *Opt. Commun.* **2018**, *407*, 17.
[45] A. B. Evlyukhin, C. Reinhardt, E. Evlyukhin, B. N. Chichkov, *J. Opt. Soc. Am. B* **2013**, *30*, 2589.
[46] A. B. Evlyukhin, B. N. Chichkov, *Physical Review B* **2019**, *100*, 125415.
[47] R. I. Woodward, R. T. Murray, C. F. Phelan, R. E. P. de Oliveira, T. H. Runcorn, E. J. R. Kelleher, S. Li, E. C. de Oliveira, G. J. M. Fechine, G. Eda, C. J. S. de Matos, *2D Mater.* **2016**, *4*, 011006.
[48] F. Yi, M. Ren, J. C. Reed, H. Zhu, J. Hou, C. H. Naylor, A. C. Johnson, R. Agarwal, E. Cubukcu, *Nano Lett.* **2016**, *16*, 1631.
[49] J. K. Day, M.-H. Chung, Y.-H. Lee, V. M. Menon, *Opt. Mater. Express* **2016**, *6*, 2360.
[50] F. J. Löchner, A. George, K. Koshelev, T. Bucher, E. Najafidehaghani, A. Fedotova, D.-Y. Choi, T. Pertsch, I. Staude, Y. Kivshar, A. Turchanin, F. Setzpfandt, *ACS Photonics* **2020**, *8*, 218.
[51] M. Nauman, J. Yan, D. de Ceglia, M. Rahmani, K. Z. Kamali, C. D. Angelis, A. E. Miroshnichenko, Y. Lu, D. N. Neshev, *Nat. Commun.* **2021**, *12*, 1.
[52] N. Kumar, S. Najmaei, Q. Cui, F. Ceballos, P. M. Ajayan, J. Lou, H. Zhao, *Phys. Rev. B* **2013**, *87*, 161403.
[53] E. Melik-Gaykazyan, K. Koshelev, J.-H. Choi, S. S. Kruk, A. Bogdanov, H.-G. Park, Y. Kivshar, *Nano Lett.* **2021**, *21*, 1765.
[54] M. K. Kroychuk, A. S. Shorokhov, D. F. Yagudin, D. A. Shilkin, D. A. Smirnova, I. Volkovskaya, M. R. Shcherbakov, G. Shvets, A. A. Fedyanin, *Nano Lett.* **2020**, *20*, 3471.